High-Precision Parallel Graphic Equalizer

Jussi Rämö, Vesa Välimäki, *Senior Member, IEEE*, and Balázs Bank, *Member, IEEE*

Abstract—This paper proposes a high-precision graphic equalizer based on second-order parallel filters. Previous graphic equalizers suffer from interaction between adjacent band filters, especially at high gain values, which can lead to substantial errors in the magnitude response. The fixed-pole design of the proposed parallel graphic equalizer avoids this problem, since the parallel second-order filters are optimized jointly. When the number of pole frequencies is twice the number of command points of the graphic equalizer, the proposed non-iterative design matches the target curve with high precision. In the three example cases presented in this paper, the proposed parallel equalizer clearly outperforms other non-iterative graphic equalizer designs, and its maximum global error is as low as 0.00–0.75 dB when compared to the target curve. While the proposed design has superior accuracy, the number of operations in the filter structure is increased only by 23% when compared to the second-order Regalia–Mitra structure. The parallel structure also enables the utilization of parallel computing hardware, which can nowadays easily outperform the traditional serial processing. The proposed graphic equalizer can be widely used in audio signal processing applications.

Index Terms—Acoustic signal processing, audio systems, digital signal processing, equalizers, infinite impulse response (IIR) filters.

I. INTRODUCTION

EQUALIZERS are a common part of modern audio systems. They were originally used to flatten, i.e., to equalize, telephone and audio systems. With telephones using fixed equalizers to enhance the intelligibility of the speech signal was adequate, but the need for an adjustable equalizer emerged in the 1930s when a recorded soundtrack was included in motion pictures [1].

Nowadays the goal of equalizing is not necessarily to flatten out the response of an audio system but rather to correct or enhance the performance of the system [2]. This includes, e.g., the correction of a loudspeaker response [3]–[5] and the loudspeaker-room interaction [6]–[10], equalization of active as well as passive headphones to assure natural music listening [11]–[14] and hear-through [15]–[17] experiences when using headphones, and enhancement of recorded music [18], [19].

A basic common equalizer is called a tone control. Tone controls can be found in many commercial audio products, and, at its simplest, it allows the user to adjust the level of bass and treble with two shelving filters [20]. When more than two filters are combined in a tone control system, which is common, e.g., in musical instrument amplifiers [21], [22], the user's possibilities to modify the sound are increased.

There are two main types of equalizers. When the user can control the gain, center frequency, and bandwidth of the equalizer filters separately, the equalizer is called a parametric equalizer [23]–[27]. A parametric equalizer is flexible and the user has good control of it, but it is quite cumbersome to use requiring an expert user, such as an audio engineer or a music producer, and it usually has a limited number of filters that the user can adjust.

A graphic equalizer, on the other hand, is much simpler to use than a parametric equalizer, since the only user-controllable parameters are the gains. The center frequencies and bandwidths of the equalizer filters, or band filters, are fixed, and the command gains are usually adjusted using sliders [28]–[30]. The sliders then plot the approximate magnitude frequency response of the equalizer, hence the name 'graphic equalizer'. Typically, a graphic equalizer has more bands, i.e., equalizer filters, than a parametric equalizer. Although the flexibility of a graphic equalizer is not as good as that of a parametric equalizer, it is often a preferred choice in sound enhancement.

A graphic equalizer can be implemented using a cascade [23], [29], [31] or a parallel [28], [30], [32] filter structure. In a cascade implementation, each band filter adjusts its magnitude response around its center frequency according to the command gain, but the magnitude response of the band filter remains close to unity, i.e., 0 dB, elsewhere. In a parallel implementation, each band filter produces a resonance at its center frequency and has a low gain at other center frequencies. Both types of equalizers suffer from interaction between adjacent band filters, which can cause substantial errors in the magnitude response [31]–[33].

This paper presents a novel idea to utilize an optimized parallel filter as a graphic equalizer. The fixed-pole design of second-order parallel filters was first presented in [34] as a means of providing efficient filtering with logarithmic frequency resolution, which is often required in audio applications [35], [36]. The use of parallel filters in our context is motivated by the fact that it provides better efficiency compared to alternative methods, including warped [37] and Kautz filters [38], as demonstrated in [39], [40].

An additional benefit of the parallel structure is the possibility to implement the equalization filters using a graphic processing unit (GPU) instead of a central processing unit (CPU) [41]. GPUs have a large number of parallel computing cores, and they have been recently used to perform audio signal processing as well, since they can outperform a CPU in many parallelizable tasks [42].

J. Rämö and V. Välimäki are with the Department of Signal Processing and Acoustics, School of Electrical Engineering, Aalto University, 02150 Espoo, Finland (e-mail: jussi.ramo@aalto.fi; vesa.valimaki@aalto.fi).

B. Bank is with the Department of Measurement and Information Systems, Budapest University of Technology and Economics, 1117 Budapest, Hungary (e-mail: bank@mit.bme.hu).
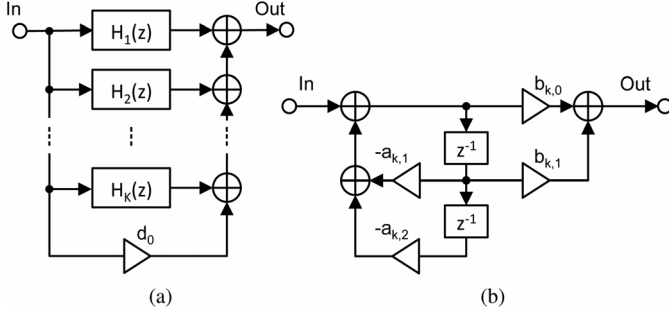
Fig. 1. Structure of (a) the parallel filter and (b) the block diagram of the second-order filter $H_k(z)$.

This paper is organized as follows. Section II describes the parallel filter design, Section III introduces the proposed parallel graphic equalizer, Section IV evaluates the performance of the parallel graphic equalizer as well as compares it to previous graphic equalizer designs, and Section V concludes this paper.

II. PARALLEL FILTER WITH FIXED POLES

The fixed-pole design of second-order parallel filters utilized in the proposed graphic equalizer was first introduced by Bank in 2007 [34]. The filter structure is depicted in Fig. 1, where (a) shows the parallel composition of the filter and (b) shows the block diagram of the kth second-order section. While the general form of the parallel filter includes an optional parallel FIR path [39], it is omitted here (see Fig. 1a), since it is not utilized in this paper. Therefore, the transfer function of the reduced parallel filter becomes

$$H(z) = d_0 + \sum_{k=1}^{K} \frac{b_{k,0} + b_{k,1}z^{-1}}{1 + a_{k,1}z^{-1} + a_{k,2}z^{-2}} \qquad (1)$$

where K is the number of second-order sections and d_0 is the gain for the parallel direct path.

Traditionally, parallel second-order filters are obtained from a high-order transfer function via partial fraction expansion. This requires first designing a high-order IIR filter followed by a conversion step. Note, however, that the high pole density at low frequencies which is required for logarithmic frequency resolution cannot be achieved with direct-form IIR filters even at double precision floating point arithmetic. As a result, the above two-step design is unfeasible in our case. This is overcome by the fixed-pole design of parallel filters, where the filter is designed in its final implementation form, and no conversion takes place.

The basic ideas of the fixed-pole parallel filter design are that the poles of the filter are constant and they form mutually linearly independent transfer functions. Then the filter design problem becomes linear in its free parameters [38]. The motivation for fixing the poles is to pre-define the frequency resolution of the filter design.

The parallel structure shown in Fig 1(a) can also be efficiently implemented by using a GPU, since all the processing blocks have the same input which are then individually processed. However, the feedback loop of the IIR filter limits the total parallelization of the structure. Nevertheless, each second-order filter can be run simultaneously in a separate core of the GPU [41].

A. Pole Positioning

The first step of the filter design is determining the pole positions. As shown in [43], the frequency resolution of the design is directly proportional to the pole frequency differences. For example, setting the pole frequencies evenly on a logarithmic scale produces logarithmic (fractional octave) resolution. While the exact values of the pole frequencies are not critical (only their distance matters), it is a straightforward choice to set the poles based on the center frequencies of the equalizer (see Sec. III-B).

Interestingly, the choice of pole radii does not noticeably alter the final filter response as long as there is sufficient overlap between the responses. A reasonable choice is to set the pole radii $|p_k|$ such that the transfer functions of the parallel sections cross approximately at their -3 dB point [43], achieved by the following formulas:

$$\theta_k = \frac{2\pi f_k}{f_s} \qquad \text{for} \ \ k = 1, 2, 3, \ldots, K, \qquad (2a)$$

$$p_k = e^{-\frac{\Delta\theta_k}{2}} e^{\pm j\theta_k}, \qquad (2b)$$

where θ_k are the pole frequencies in radians given by the predetermined analog frequency series f_k and the sampling frequency f_s. The bandwidth of the kth second-order section $\Delta\theta_k$ is computed from the neighboring pole frequencies:

$$\Delta\theta_k = \frac{\theta_{k+1} - \theta_{k-1}}{2} \ \ \text{for} \ \ k = 2, 3, \ldots, K-1,$$
$$\Delta\theta_1 = \theta_2 - \theta_1,$$
$$\Delta\theta_K = \theta_K - \theta_{K-1}. \qquad (3)$$

The denominator coefficients of the transfer function $a_{k,1}$ and $a_{k,2}$ are derived from the poles p_k as follows:

$$a_{k,1} = -\left(p_k + \overline{p}_k\right) = -2|p_k|\cos\theta_k, \qquad (4a)$$
$$a_{k,2} = |p_k|^2, \qquad (4b)$$

where $\overline{p}_k$ is the complex conjugate of p_k.

B. Design of the Numerator Part

Once the denominator coefficients are determined from the poles, the problem becomes linear in its free numerator parameters $b_{k,0}$, $b_{k,1}$, and d_0, which are seen in Fig. 1.

Writing (1) in matrix form for a finite set of angular frequencies ω_n ($n = 1, 2, \ldots, N$) yields

$$\mathbf{h} = \mathbf{M}\mathbf{p}, \qquad (5)$$

where $\mathbf{p} = [b_{1,0}, b_{1,1}, \ldots, b_{K,0}, b_{K,1}, d_0]^T$ is a column vector comprising the free parameters. The columns of the modeling matrix $\mathbf{M}$ contain the frequency responses of the second-order denominators $1/(1 + a_{k,1}e^{-j\omega_n} + a_{k,2}e^{-j2\omega_n})$ and their delayed versions $e^{-j\omega_n}/(1 + a_{k,1}e^{-j\omega_n} + a_{k,2}e^{-j2\omega_n})$ for the angular frequencies ω_n. The last column of $\mathbf{M}$ belongs to the direct path gain d_0, and thus all of its elements are 1. Finally, $\mathbf{h} = [H(\omega_1) \ldots H(\omega_N)]^T$ is a column vector containing the resulting frequency response.

Now the task is to find the optimal parameters $\mathbf{p}_{\text{opt}}$ such that $\mathbf{h} = \mathbf{M}\mathbf{p}_{\text{opt}}$ is closest to the target frequency response $\mathbf{h}_{\text{t}} = [H_{\text{t}}(\omega_1) \ldots H_{\text{t}}(\omega_N)]^T$. If the error is evaluated in the

mean squares sense, the minimum is found by the well known least-squares (LS) solution

$$\mathbf{p}_{\mathrm{opt}} = \mathbf{M}^{+}\mathbf{h}_{\mathrm{t}}, \tag{6a}$$

$$\mathbf{M}^{+} = (\mathbf{M}^{H}\mathbf{M})^{-1}\mathbf{M}^{H}, \tag{6b}$$

where $\mathbf{M}^{+}$ is the Moore-Penrose pseudo-inverse and $\mathbf{M}^{H}$ is the conjugate transpose of $\mathbf{M}$. Note that this method is very similar to the LS FIR filter except that the modeling matrix M now contains the frequency responses of the second-order denominators instead of, for example, cosine terms, which are used in linear-phase FIR filter design [44]. When the frequency resolution—the set of poles and the modeling matrix $\mathbf{M}$—is fixed, which is the case for a graphic equalizer, the pseudo-inverse $\mathbf{M}^{+}$ can be precomputed and stored. As a result, the parameter estimation reduces to the matrix multiplication in (6a), reducing design time [43].

Note that (6) assumes a filter specification $H_{\mathrm{t}}(\omega_n)$ given for the full frequency range $\omega_n \in [-\pi, \pi]$ and thus allows designing filters with complex coefficients. However, in our case, we are interested in filters with a real impulse response, that is, having a conjugate-symmetric frequency response, which allows the reduction of computational complexity in (6). In this case, a real modeling matrix $\mathbf{M}_{\mathrm{r}}$ is formed by placing the real and imaginary parts of the complex matrix $\mathbf{M}$ in tandem for frequencies $\omega_n \in [0, \pi]$, as also for the real target vector $\mathbf{h}_{\mathrm{t,r}}$:

$$\mathbf{M}_{\mathrm{r}} = \begin{bmatrix} \mathrm{Re}\{\mathbf{M}\} \\ \mathrm{Im}\{\mathbf{M}\} \end{bmatrix}, \tag{7a}$$

$$\mathbf{h}_{\mathrm{t,r}} = \begin{bmatrix} \mathrm{Re}\{\mathbf{h}_{\mathrm{t}}\} \\ \mathrm{Im}\{\mathbf{h}_{\mathrm{t}}\} \end{bmatrix}. \tag{7b}$$

The optimal set of numerator parameters is thus obtained from

$$\mathbf{p}_{\mathrm{opt}} = \mathbf{M}_{\mathrm{r}}^{+}\mathbf{h}_{\mathrm{t,r}}, \tag{8a}$$

$$\mathbf{M}_{\mathrm{r}}^{+} = (\mathbf{M}_{\mathrm{r}}^{T}\mathbf{M}_{\mathrm{r}})^{-1}\mathbf{M}_{\mathrm{r}}^{T}, \tag{8b}$$

which now only involves real multiplications.

C. Frequency-Dependent Weighting

The frequency points can also be assigned different weights during LS error minimization [36], [44], in which case the error is

$$e_{\mathrm{WLS}} = \sum_{n=1}^{N} W(\omega_n)|H(e^{\mathrm{j}\omega_n}) - H_{\mathrm{t}}(\omega_n)|^2, \tag{9}$$

where $W(\omega_n)$ is a non-negative weight for frequency ω_n. The computationally most efficient implementation of weighting in parameter estimation is to multiply all the elements of the modeling matrix $\mathbf{M}_{\mathrm{r}}$ and target vector $\mathbf{h}_{\mathrm{t,r}}$, which correspond to frequency ω_n, by $\sqrt{W(\omega_n)}$ before computing (8). Note that if the weights depend on the target response $H_{\mathrm{t}}(\omega_n)$, the pseudo-inverse $\mathbf{M}_{\mathrm{r}}^{+}$ cannot be precomputed, but it must be evaluated when the target response is changed.

III. PARALLEL GRAPHIC EQUALIZER

This section demonstrates the effectiveness of the parallel filters from Sec. II for designing a highly accurate graphic equalizer.

A. Target Computation

The graphic equalizer design starts with computing a target frequency response based on the command gains G_m of the graphic equalizer at frequencies $f_{c,m}$ for $m = 1, 2, \ldots, P$, where P is the number of command points. To this end, the magnitude response is first computed using a suitable interpolation from the command points so that a smooth curve is produced between the command points with no overshoots. Hermite and spline interpolation are two potential methods for obtaining a smooth target magnitude response [45]. They both produce an interpolating function, which not only matches the given data points but also some of the derivatives of the data.

The cubic Hermite and spline interpolation methods fit the interpolating function to the data and its slope at the known points. In our examples, the target magnitude response was computed on a logarithmic frequency grid ($10P$ frequency points) on a decibel scale by using the piecewise Hermite cubic interpolation readily available in MATLAB (the `pchip` function). The `pchip` function is preferred over `spline` in MATLAB, because `spline` can produce significant overshoots between command points when the input data are non-smooth.

Next, a suitable phase response has to be generated, since a complex target $H_{\mathrm{t}}(\omega_n)$ is required by the LS design of Sec. II-B. Minimum phase is a natural choice, since analog graphic equalizers also have minimum phase [46]. In addition, the energy of a minimum-phase system is concentrated near the beginning of the impulse response [47], which makes it easy to model with parallel filters, since the impulse response of parallel filters is a linear combination of decaying sinusoidal functions. Notice that, for example, a linear-phase response would be particularly difficult to model with parallel filters.

Therefore, a phase response is computed corresponding to a minimum-phase transfer function. For this, the magnitude response is first resampled to a linear frequency scale (2^{15} frequency points) and its logarithm is computed. Next, the Hilbert transform of the log magnitude is computed with the help of an FFT and IFFT operation, and this gives the phase response [48]. Finally, the linear-frequency-scale phase data is sampled at the original logarithmic frequency points.

B. Parallel Graphic Equalizer Design

The first step of the filter design is setting up the pole frequencies. A straightforward choice for the pole frequencies is setting them equal to the center frequencies of the command points. However, doing so results in a large approximation error if the command points alternate between $+12$ dB and -12 dB, because this would require a higher Q value than is possible with such a small number of poles. This can be seen in Fig. 2(a) around 500 Hz for a third-octave equalizer example. The maximum magnitude of the error in Fig. 2(a) is more than 15 dB near 1 kHz. Fig. 2(a) also shows that with more reasonable equalizer settings, such as those used below 400 Hz, even this low number of poles provides an acceptable performance.

The biggest problems in Fig. 2(a) are in those regions where the command gains are at the lowest level. This is because in normal LS design the error is minimized in the linear scale, and the same linear error means a larger error in dB whenever the target is smaller. This problem can be overcome by
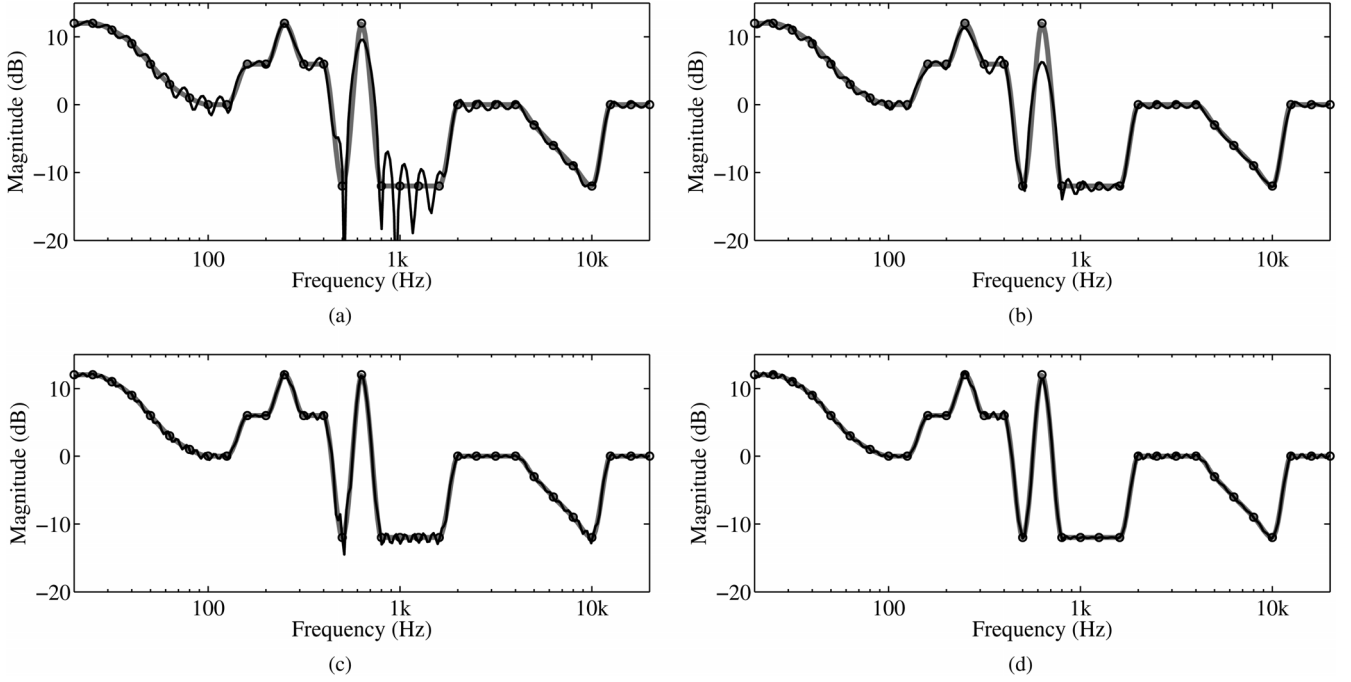
Fig. 2. Parallel equalizer design examples using same number of pole frequencies as center frequencies (a) without and (b) with frequency-dependent weighting, and using double number of pole frequencies (c) without and (d) with frequency-dependent weighting. The parameters for cases (a) and (b) are $P = 31$, $K = 31$, $N = 62$, and the total filter order of 62; and for cases (c) and (d) $P = 31$, $K = 62$, $N = 124$, and the total filter order is 124. The command points are displayed by circles, and the interpolated target response is shown by a gray line. The sample rate is 44.1 kHz.

TABLE I
CENTER FREQUENCIES (f_c) AND BANDWIDTHS (f_B) FOR THE SECOND-ORDER REGALIA-MITRA FILTERS IN HERTZ

Band	1	2	3	4	5	6	7	8	9	10	11	12	13	14	15	16
f_c	20	25	31.5	40	50	63	80	100	125	160	200	250	315	400	500	630
f_B	2.3	2.9	3.6	4.6	5.8	7.3	9.3	11.6	14.5	18.5	23.2	28.9	36.5	46.3	57.9	72.9
Band	17	18	19	20	21	22	23	24	25	26	27	28	29	30	31	
f_c	800	1000	1250	1600	2000	2500	3150	4000	5000	6300	8000	10000	12500	16000	20000	
f_B	92.6	116	145	185	232	290	365	463	579	730	926	1158	1447	1853	2316	

applying an appropriate weighting $W(\omega_n) = 1/|H_t(\omega_n)|^2$, scaling the target and filter responses in the error function (9) by $1/|H_t(\omega_n)|$ so that they will be all in the same range (actually, around unity in magnitude). Note that the square is required in the weighting function since $W(\omega_n)$ is not squared in (9). Fig. 2(b) shows that weighting improves the performance significantly, and the error is more evenly distributed on the dB scale. However, the sharp peak around 600 Hz is still poorly modeled.

The accuracy can be improved by increasing the number of poles and thus the corresponding Q values. We have found that having twice the number of pole frequencies as the number of band frequencies (i.e., $K = 2P$) is a sufficient compromise between accuracy and efficiency for a ±12-dB graphic equalizer even with the hardest command settings, since the maximum error remains smaller than 1 dB. In this case the pole frequencies are simply chosen as the band center frequencies, and the additional pole frequencies are inserted at 10 Hz and at each band edge. Thus, the pole frequencies f_k used in Figs. 2(c) and 2(d) are 10 Hz, $f_{c,1}$, $f_{U,1}$, $f_{c,2}$, $f_{U,2}$, $f_{c,3}$, ..., $f_{U,30}$, and $f_{c,31}$. The values of f_c and f_U are shown in Tables I and II, respectively.

The magnitude response shown in Fig. 2(c) is for the equalizer without weighting (maximum error 3.1 dB) and in Fig. 2(d) with weighting $W(\omega_n) = 1/|H_t(\omega_n)|^2$ (maximum error 0.66 dB). While the frequency weighting leads to a better frequency response, the advantage of the non-weighted design is that, in this case, the pseudo-inverse $\mathbf{M}_r^+$ can be precomputed, as discussed in Sec. II-B. The choice between these two options must depend on the application, namely, on how often the command points are changed by the user.

Note that the design complexity is linearly proportional to the number of target frequency points, i.e., the length of $\mathbf{h}_{t,r}$ in (8a). Generally, the number of frequency points must be larger than the filter order, because otherwise the response may oscillate between them [44]. Again, more frequency points result in better accuracy. In our experience, sampling the target frequency response at twice the number of points as the pole frequency number is a reasonable compromise, since increasing this number further does not significantly improve accuracy. Therefore, this choice has been used in all the examples of the paper. Thus, in the third-octave equalizer, the number of pole frequencies and target frequency points are 62 and 124, respectively.
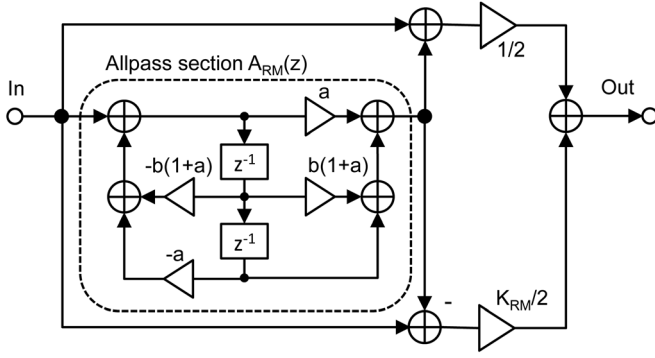
Fig. 3.   Block diagram of a second-order Regalia-Mitra equalizer filter.

IV. EVALUATION

This section evaluates the performance of the third-octave parallel graphic equalizer (PGE) and compares it against a commercial analog graphic equalizer as well as two previously known digital graphic equalizer designs, a second-order Regalia-Mitra (RM) [23] filter and a higher-order filter design introduced by Holters and Zölzer [29]. The second-order RM-based graphic equalizer was chosen because the RM filters have been traditionally used in equalization [49]–[52]. Furthermore, the high-order graphic equalizer has been selected for our comparison, since it is a recent design which enables the implementation of a more precise graphic equalizer than that based on second-order sections [29], [53]. Both of the filters can be used in non-iterative graphic equalizer designs. All digital filters used in this comparison run at the sample rate of 44.1 kHz.

The analog graphic equalizer used in this comparison is a commercial 31-band stereo graphic equalizer whose band filters are active minimum-phase RC networks. The performance was evaluated by measuring the impulse response of the equalizer using the sine-sweep technique [54].

A. Digital Second-Order Equalizer

A digital second-order equalizer, which is implemented using tunable RM equalization filters [23] with symmetric notch correction [55], is presented in this section. It provides adjustable gain to a given band while it leaves the rest of the spectrum untouched. Fig. 3 shows the block diagram of the RM equalization filter. The transfer function of the filter is [23]

$$H(z) = \frac{1}{2}[1 + A_{\mathrm{RM}}(z)] + \frac{K_{\mathrm{RM}}}{2}[1 - A_{\mathrm{RM}}(z)], \qquad (10)$$

where K_{RM} is the gain of the filter and $A_{\mathrm{RM}}(z)$ is an allpass filter with the transfer function

$$A_{\mathrm{RM}}(z) = \frac{a + b(1+a)z^{-1} + z^{-2}}{1 + b(1+a)z^{-1} + az^{-2}}. \qquad (11)$$

The frequency parameter a for a peak ($K_{\mathrm{RM}} \geq 1$) and notch ($K_{\mathrm{RM}} < 1$) filter is specified as [23], [55]

$$a = \begin{cases} \frac{1 - \tan(\Omega/2)}{1 + \tan(\Omega/2)}, & \text{when } K_{\mathrm{RM}} \geq 1, \\[2mm] \frac{K_{\mathrm{RM}} - \tan(\Omega/2)}{K_{\mathrm{RM}} + \tan(\Omega/2)}, & \text{when } K_{\mathrm{RM}} < 1, \end{cases} \qquad (12)$$

where Ω is the normalized filter bandwidth. The parameter b in (11) is set as

$$b = -\cos(\omega_0), \qquad (13)$$

where ω_0 is the normalized center frequency [23]. The normalized center frequencies and bandwidths are calculated as follows:

$$\omega_0 = 2\pi f_{\mathrm{c}}/f_{\mathrm{s}}, \qquad (14\mathrm{a})$$
$$\Omega = 2\pi f_{\mathrm{B}}/f_{\mathrm{s}}, \qquad (14\mathrm{b})$$

where f_{c}, the center frequency; f_{B}, the bandwidth of the filter; and f_{s}, the sampling rate, are all in hertz.

When the user of the graphic RM equalizer sets the gain K_{RM} to less than one, the parameter a for that band must be recalculated using (12). However, when the gain remains at a value of one or higher, only the gain parameter K_{RM} is updated.

B. Digital High-Order Equalizer

The digital high-order graphic equalizer is based on the filter structure presented by Orfanidis [56] and the high-order graphic equalizer design introduced by Holters and Zölzer [29]. The high-order graphic equalizer consists of fourth-order sections that can be cascaded in order to create high-order minimum-phase filters for each band. The high-order filters can create exceptionally steep transition bands, thus making the adjacent filters almost independent of each other. We have previously used the high-order filters to implement a Bark-band graphic equalizer that provides an accurate control of each individual Bark band [13], [53].

Fig. 4 shows the block diagram of the mth fourth-order section of the high-order graphic equalizer, where

$$\alpha_m = (\frac{1}{2} - \frac{2m-1}{2M})\pi, \qquad (15)$$
$$c_m = \cos(\alpha_m), \qquad (16)$$
$$V = \sqrt[M]{g} - 1, \qquad (17)$$

$2M$ is the filter order, and g is the desired gain. Furthermore,

$$K_{\mathrm{EQ4}} = \frac{1}{\sqrt[2M]{g}} \tan(\frac{\Omega_{\mathrm{B}}}{2}), \qquad (18)$$

where Ω_{B} is the normalized filter bandwidth and

$$a_{0,m}^{-1} = \frac{1}{1 + 2K_{\mathrm{EQ4}}c_m + K_{\mathrm{EQ4}}^2}. \qquad (19)$$

$A(z)$ is a second-order allpass filter having the transfer function

$$A(z) = \frac{\cos(\Omega_{\mathrm{M}})z^{-1} + z^{-2}}{1 + \cos(\Omega_{\mathrm{M}})z^{-1}}, \qquad (20)$$

where Ω_{M} is the optimized and normalized center frequency

$$\Omega_{\mathrm{M}} = 2\arctan\sqrt{\tan(\frac{\Omega_{\mathrm{U}}}{2})\tan(\frac{\Omega_{\mathrm{L}}}{2})}, \qquad (21)$$

and Ω_{L} and Ω_{U} are the normalized lower and upper cut-off frequency of the filter, respectively. The normalized cut-off frequencies are obtained as follows:

$$\Omega_{\mathrm{L}} = 2\pi f_{\mathrm{L}}/f_{\mathrm{s}}, \qquad (22\mathrm{a})$$
$$\Omega_{\mathrm{U}} = 2\pi f_{\mathrm{U}}/f_{\mathrm{s}}. \qquad (22\mathrm{b})$$

TABLE II
LOWER (f_L) AND UPPER (f_U) CUTOFF FREQUENCIES FOR THE FOURTH-ORDER FILTERS IN HERTZ

Band	1	2	3	4	5	6	7	8	9	10	11	12	13	14	15	16
f_L	17.5	22.4	28.2	35.5	44.7	56.2	70.8	89.1	112	141	178	224	282	355	447	562
f_U	22.4	28.2	35.5	44.7	56.2	70.8	89.1	112	141	178	224	282	355	447	562	708

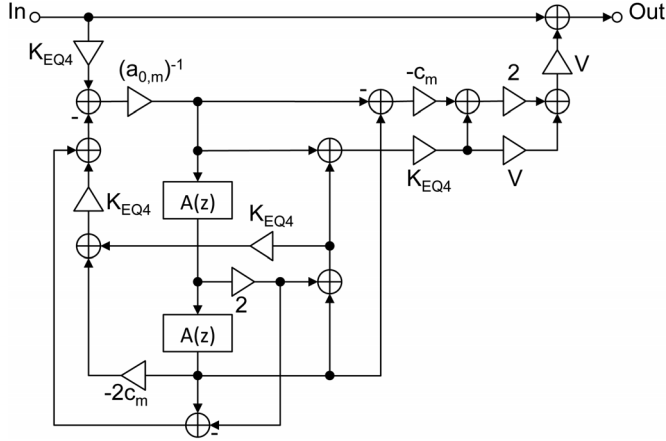| Band	17	18	19	20	21	22	23	24	25	26	27	28	29	30	31	
f_L	708	891	1120	1410	1780	2240	2820	3550	4470	5620	7080	8910	11200	14100	17800	
f_U	891	1120	1410	1780	2240	2820	3550	4470	5620	7080	8910	11200	14100	17800	22050	

Fig. 4. Block diagram of mth fourth-order section of the EQ4 graphic equalizer [29], [53].

When the gain g of the high-order graphic equalizer is altered in some band, parameters V, K_{EQ4}, and $a_{0,m}^{-1}$ must be recalculated for each fourth-order section used in that band using (17), (18), and (19), respectively.

C. Equalizer Parameters

Digital Second-Order RM Equalizer: The used third-octave center frequencies f_c and bandwidths f_B of the RM filters in hertz are shown in Table I. The used bandwidths are half of the typical third-octave filter bandwidths. The bandwidth of the filters was manually chosen such that the results are the best compromise in all example cases. Increasing the bandwidths increases the interaction between the adjacent filters, which results in larger errors at the center frequencies, and decreasing the bandwidths decreases the interaction between the filters, which may decrease the maximum errors at the center frequencies but increases the global error. The center frequencies and bandwidths of the RM equalizer were normalized using (14a) and (14b).

Digital fourth-order EQ4 Equalizer: Table II shows the lower and upper cut-off frequencies of the fourth-order filters in hertz. The lower and upper cut-off frequencies were normalized using (22a) and (22b) whereas the optimized and normalized center frequencies were calculated using (21). In this comparison we use only one fourth-order section per band (see Fig. 4) so that the total filter order compared to the proposed parallel implementation is approximately the same.

D. Accuracy

Figs. 5–7 show the magnitude responses of the four graphic equalizers that are compared. Every figure has four subfigures,

where (a) is the analog equalizer, (b) is the second-order RM, (c) is the fourth-order EQ4, and (d) is the proposed PGE. Furthermore, the thick gray line is the target curve, and it is the same in the four subfigures within every figure. The circles indicate the commands, i.e., the slider positions G_m of the graphic equalizer, and the black line is the magnitude response of the equalizer being evaluated. Furthermore, the number of the commands P is 31 in all cases (a)–(d). Thus, the filter order of the RM equalizer (b) is 62, because it consists of 31 second-order filters. For the EQ4 (c), the filter order is 124, since it consists of 31 fourth-order sections. For the PGE (d), the order of the denominator is 124, but the order of the numerator is 62.

Fig. 5 shows an extreme example where all of the commands are set to $+12$ dB, which is also the maximum gain of the analog equalizer. This example reveals the weakness of the analog and digital low-order graphic equalizers in Figs. 5(a) and 5(b), respectively. Since the individual sub-band filters are reasonably wide, the errors are rather drastic when they are summed up. However, when the order of the filters is increased, as in the case of Fig. 5(c), the errors due to the interaction of the filters are decreased. As can be seen, the fourth-order equalizer in Fig. 5(c) still has a slight overshoot (less than 2 dB) around the filter center frequencies, whereas the proposed parallel equalizer in Fig. 5(d) easily achieves the target curve with zero errors with the help of the parallel direct path gain d_0 (see Sec. II). Although this kind of command setting is not typical for graphic equalizers, it demonstrates the flexibility of the proposed parallel graphic equalizer.

Fig. 6 shows an example where the commands are in a zigzag formation, with the gains alternating between ± 12 dB. As can be seen in Figs. 6(a) and 6(b), the filter responses do not reach the set command points due to the low filter order, whereas fourth-order equalizer in Fig. 6(c) almost reaches target values (the error is about 2 dB). The response of the proposed parallel implementation presented in Fig. 6(d), however, has no problem reaching all of the command points with good accuracy, as the maximum error is 0.75 dB.

Fig. 7 shows an example where every third command is set to $+12$ dB and the rest remain at 0 dB. This example demonstrates the overlapping of the neighboring equalizer filters. As can be seen in Figs. 7(a) and 7(b), the low-order band filters are so wide that even when only every third band filter is in use, they interact and raise the response between the peaks by approximately 4–6 dB. Again, when the order of the filters is increased, as for Fig 7(c), the interaction between adjacent filters becomes smaller and the overall response is more accurate. Yet again, the response of the parallel implementation shown in Fig. 7(d) has
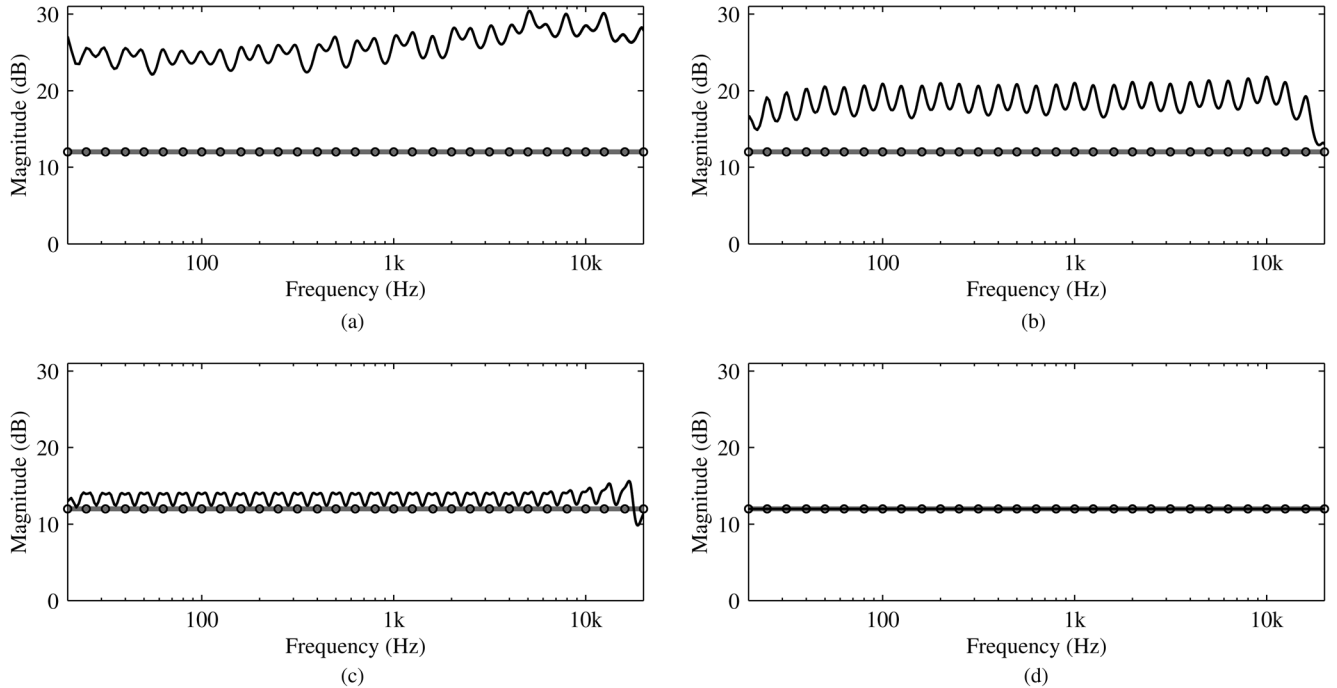
Fig. 5.   Magnitude response of different graphic equalizers when the commands are all up (+12 dB). (a) is the response of the analog equalizer, (b) is the response of the second-order RM equalizer, (c) is that of the fourth-order EQ4, and (d) is that of the proposed parallel equalizer PGE. The thick gray line is the target curve, and the circles indicate the command positions.
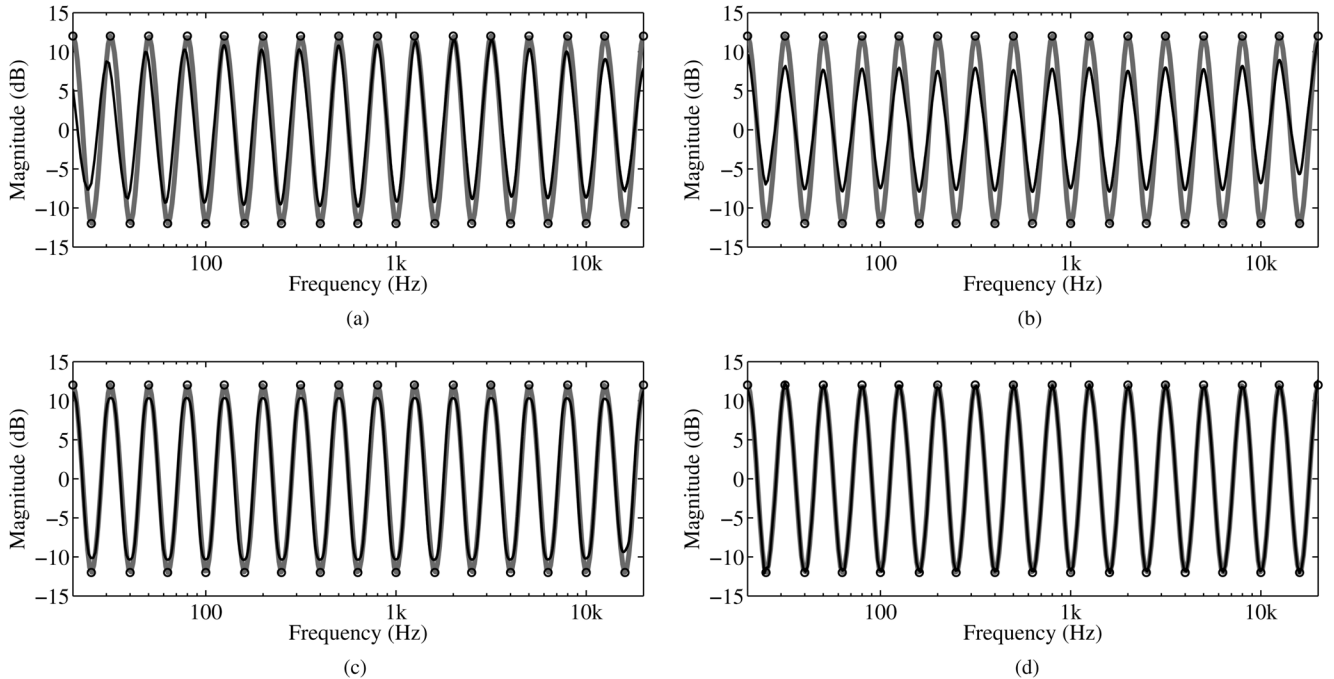

Fig. 6.   Magnitude response with zigzag command settings (±12 dB) for (a) the analog equalizer, (b) the RM equalizer, (c) the EQ4 equalizer, and (d) the proposed PGE.

the most accurate response when compared to the target curve, with a maximum error of 0.32 dB.

Table III shows the maximum errors of the equalizer responses in Figs. 5–7 compared to the target curve in the audible range of 20 Hz to 20 kHz. As can be seen, the performance of the proposed PGE is clearly the best in terms of maximum error. Furthermore, the numbers in parentheses show the maximum errors of the PGE without frequency-dependent weighting. As can be seen in Table III, the errors without the weighting are com-

parable to those obtained with weighting when the gains are set to have positive values, as in the first and last case (see Figs. 5 and 7). However, when negative gains are applied, as in the zigzag case (see Fig. 6), the maximum error in dB in the PGE with no frequency-dependent weighting increases substantially. This is related to the fact that all negative gains in dB are mapped to the linear range from 0 to 1 in the LS design (see also Sec. III-B).

We also experimented with a technique similar to that proposed by Lane *et al.* [33], where the RM equalizer command
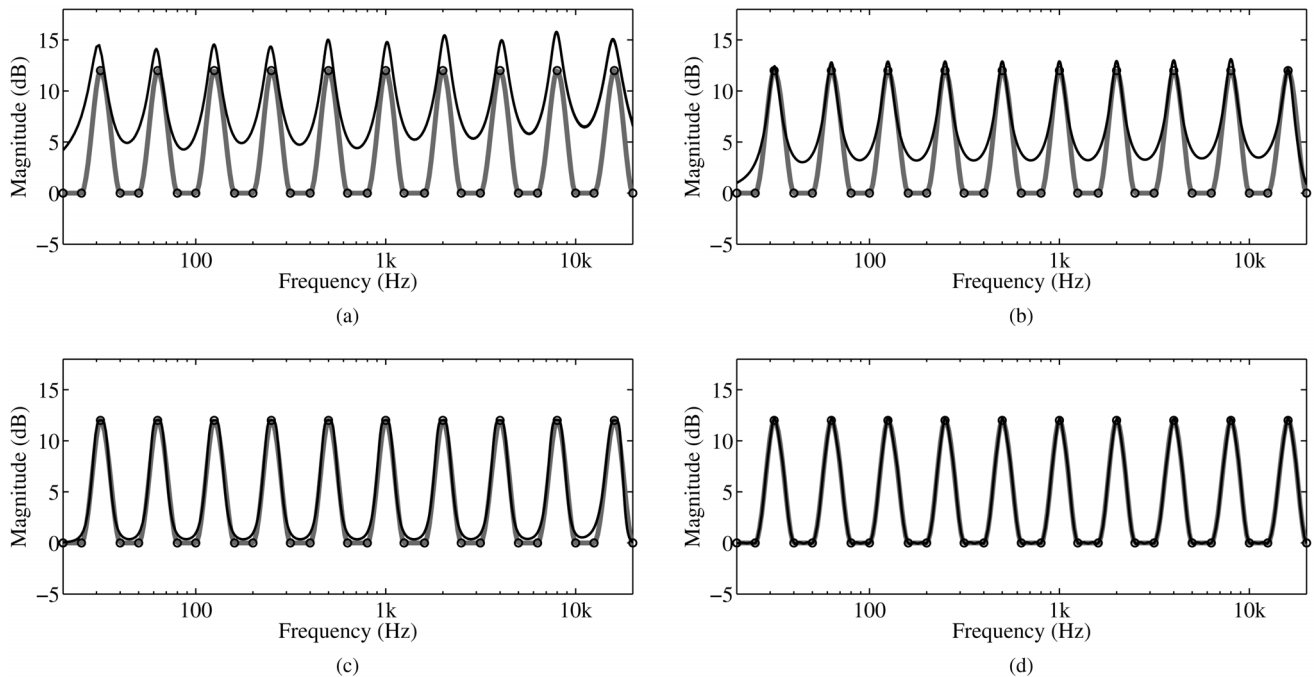
Fig. 7. Magnitude response of (a) the analog, (b) the RM, (c) the EQ4, and (d) the proposed graphic equalizer, when every third command is up (+12 dB) and the others are at zero.

TABLE III
MAXIMUM ERRORS OF THE THIRD-OCTAVE BAND EXAMPLES IN DECIBELS. THE BEST RESULT IN EACH CASE IS HIGHLIGHTED. THE NUMBERS IN PARENTHESES IN THE PGE COLUMN CORRESPOND TO THE RESULTS WITHOUT FREQUENCY-DEPENDENT WEIGHTING

Case	Analog	RM	EQ4	PGE
All up (Fig. 5)	18	9.8	3.6	**0.00 (0.00)**
Zigzag (Fig. 6)	4.4	6.3	2.8	**0.75** (2.0)
Every third up (Fig. 7)	7.5	4.1	1.5	0.32 **(0.29)**

gains are adjusted to compensate for the interaction occurring between the adjacent band filters in order to get more accurate results. This type of a technique can generally improve the result, but the EQ4 and PGE still overcome the improved second-order design in the selected example cases presented in Figs. 5–7.

Moreover, it is of interest to compare the temporal behavior of the equalizers. Fig. 8 shows the impulse responses of the four graphic equalizers when the commands are set to a zigzag formation, as in Fig. 6. As can be seen in Fig. 8, all of the impulse responses have highly similar minimum-phase characteristics, as they release most of their energy in the beginning.

E. Computational Complexity

Furthermore, the number of operations required—the additions and multiplications—during the filtering of each output sample of the three digital graphic equalizers are shown in Table IV. As can be seen, the second-order RM equalizer (see Fig. 3) has the smallest number of operations, as expected. The fourth-order EQ4 needs more than twice as many operations as the RM equalizer, because of its special structure, as shown in Fig. 4. Finally, the proposed PGE needs only 23% more operations than the RM equalizer although it contains twice as many sections. The PGE is computationally efficient, because
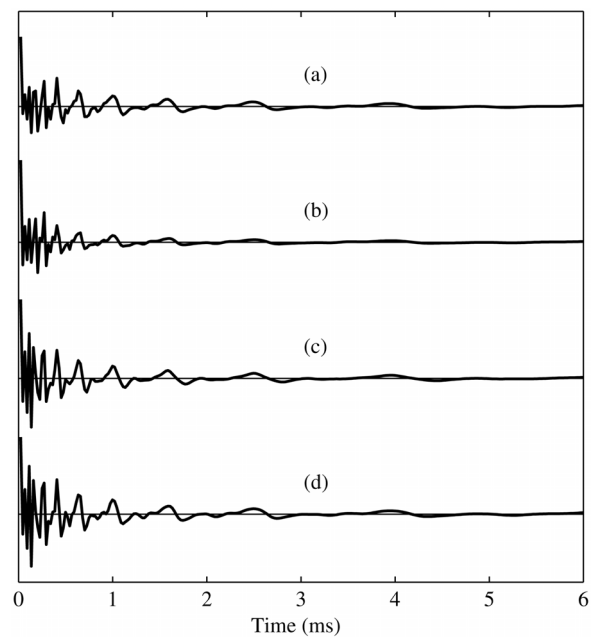

Fig. 8. Impulse responses of (a) the analog equalizer, (b) the RM equalizer, (c) the EQ4 equalizer, and (d) the proposed parallel equalizer PGE. The impulse responses correspond to Fig. 6, where the equalizer commands are set to the zigzag formation.

it consists of sections which have a second-order all-pole part and a first-order numerator part, as seen in Fig. 1(b).

One additional aspect of the graphic equalizer design is the amount of calculation necessary when the user changes a command gain of the equalizer. When a single command gain is changed, the required calculations for the different equalizers are as follows:

RM: for a positive value of the gain on a decibel scale, only the coefficient K_{RM} has to be updated. However, when the gain

TABLE IV
NUMBER OF OPERATIONS PER OUTPUT SAMPLE FOR THE DIFFERENT
TYPES OF THIRD-OCTAVE EQUALIZERS

Operation	RM	EQ4	PGE
ADD	217	434	248
MUL	186	465	249
TOTAL	403	899	497

TABLE V
AVERAGE COMMAND GAIN UPDATE TIMES IN MATLAB

RM	EQ4	PGE
0.02 ms	0.12 ms	30 ms

is changed to be negative, also (12), that includes additions, divisions, and tangent functions, has to be recalculated. The updates are done only within one band filter.

EQ4: Regardless of the value of the gain, (17), (18), and (19) have to be recalculated, which contain root and tangent functions, divisions, and additions. The updates are done only within the filter whose gain is altered. If the order of the filter is more than four, the recalculation has to be made for each fourth-order section used in that band.

PGE: The proposed PGE has heavier gain update process, since the whole set of numerators of the parallel filters are recomputed. When a gain value is changed, the target minimum-phase specification $\mathbf{h}_{t,r}$ must be recalculated. When the frequency-dependent weighting is in use, the matrix pseudo-inverse $\mathbf{M}_r^+$ is also recalculated using (8b). However, if the frequency-dependent weighting is not used, $\mathbf{M}_r^+$ can be precomputed, and thus the gain update requires only the recalculation of $\mathbf{h}_{t,r}$ and multiplications using (8a).

The gain update calculation for the PGE is heavier than that of the previous equalizers. However, it must be noted that the calculations have to be done only when the user alters a command gain. Table V show the average time that is needed for the gain update. The shown update times were calculated using MATLAB as an average of one hundred updates, when all command gains were changed to random values. As can be seen in Table V, the RM equalizer has the fastest update time (about 0.02 ms), as expected. The EQ4 has the second fastest update time (approximately 0.12 ms), while the PGE has the slowest update time (about 30 ms).

However, equalizer presets, such as classical music, rock music, and pop music settings, which are nowadays found in many consumer devices, can be easily precomputed and stored in memory. Preset settings for the PGE require only a small amount of memory, since only the numerator and d_0 have to be stored. The denominator coefficients are the same for all settings, and they are precomputed and stored in memory in any case.

V. CONCLUSION

This paper introduced a novel high-precision graphic equalizer design, which consists of parallel second-order filters. The accuracy of the proposed new parallel graphic equalizer outperforms other graphic equalizers with non-iterative design, which are typically used in audio signal processing. Furthermore, the

parallel structure of the proposed design enables the efficient use of multicore GPUs, which often have superior performance when executing parallel algorithms.

We observed that twice the number of poles as the command gains of the graphic equalizer is a good compromise between accuracy and efficiency of the system, when the gains are varied between ±12 dB. Furthermore, using frequency-dependent weighting during the error minimization also improves the accuracy of the parallel equalizer. However, when the weighting is used, it complicates the error minimization calculation, since the pseudo-inverse of the modeling matrix cannot be precomputed. Whether the frequency weighting should be included in the design or not should be decided based on the application the proposed parallel equalizer will be used for.

The results show that with weighting the parallel equalizer operates highly accurately with the given design, maintaining errors of less than 1 dB even during the hardest example cases. Although the proposed filtering can be implemented with a 45% smaller number of operations than a graphic equalizer based on fourth-order filters, the achieved accuracy is better.

A MATLAB implementation of the design method with examples is available at http://www.acoustics.hut.fi/go/ieee-taslp-pge.

REFERENCES

[1] D. A. Bohn, "Operator adjustable equalizers: An overview," in *Proc. AES 6th Int. Conf.*, May 1988, pp. 369–381.

[2] R. Berkovitz, "Digital equalization of audio signals," in *Proc. AES 1st Int. Conf.: Digital Audio*, Jun. 1982, pp. 226–238.

[3] M. Karjalainen, E. Piirilä, A. Järvinen, and J. Huopaniemi, "Comparison of loudspeaker equalization methods based on DSP techniques," *J. Audio Eng. Soc.*, vol. 47, no. 1–2, pp. 15–31, Jan/Feb 1999.

[4] A. Marques and D. Freitas, "Infinite impulse response (IIR) inverse filter design for the equalization of non-minimum phase loudspeaker systems," in *Proc. IEEE Workshop Applicat. Signal Process. Audio Acoust.*, New Paltz, NY, USA, Oct. 2005, pp. 170–173.

[5] G. Ramos and J. J. López, "Filter design method for loudspeaker equalization based on IIR parametric filters," *J. Audio Eng. Soc.*, vol. 54, no. 12, pp. 1162–1178, Dec. 2006.

[6] J. N. Mourjopoulos, "Digital equalization of room acoustics," *J. Audio Eng. Soc.*, vol. 42, no. 11, pp. 884–900, Nov. 1994.

[7] M. Karjalainen, P. A. A. Esquef, P. Antsalo, A. Mäkivirta, and V. Välimäki, "Frequency-zooming ARMA modeling of resonant and reverberant systems," *J. Audio Eng. Soc.*, vol. 50, no. 12, pp. 1012–1029, Dec. 2002.

[8] A. Mäkivirta, P. Antsalo, M. Karjalainen, and V. Välimäki, "Modal equalization of loudspeaker-room responses at low frequencies," *J. Audio Eng. Soc.*, vol. 51, no. 5, pp. 324–343, May 2003.

[9] A. Carini, S. Cecchi, F. Piazza, I. Omiciuolo, and G. L. Sicuranza, "Multiple position room response equalization in frequency domain," *IEEE Trans. Audio, Speech, Lang. Process.*, vol. 20, no. 1, pp. 122–135, Jan. 2012.

[10] B. Bank, "Loudspeaker and room equalization using parallel filters: Comparison of pole positioning strategies," in *Proc. AES 51st Int. Conf.*, Helsinki, Finland, Aug. 2013.

[11] G. Lorho, "Subjective evaluation of headphone target frequency responses," in *Proc. AES 126th Conv.*, Munich, Germany, May 2009.

[12] A. Lindau and F. Brinkmann, "Perceptual evaluation of headphone compensation in binaural synthesis based on non-individual recordings," *J. Audio Eng. Soc.*, vol. 60, no. 1/2, pp. 54–62, Jan.–Feb. 2012.

[13] J. Rämö, V. Välimäki, and M. Tikander, "Perceptual headphone equalization for mitigation of ambient noise," in *Proc. IEEE Int. Conf. Acoust., Speech, Signal Process. (ICASSP)*, Vancouver, BC, Canada, May 2013, pp. 724–728.

[14] S. E. Olive, T. Welti, and E. McMullin, "Listener preferences for in-room loudspeaker and headphone target responses," in *Proc. AES 135th Convention*, New York, NY, October 2013.

[15] M. Tikander, "Usability issues in listening to natural sounds with an augmented reality audio headset," *J. Audio Eng. Soc.*, vol. 57, no. 6, pp. 430–441, Jun. 2009.

[16] J. Rämö and V. Välimäki, "Digital augmented reality headset," *J. Elect. Comput. Eng.*, vol. 2012, 2012.

[17] J. Rämö, V. Välimäki, and M. Tikander, "Live sound equalization and attenuation with a headset," in *Proc. AES 51st Int. Conf.*, Helsinki, Finland, Aug. 2013.

[18] E. Perez Gonzales and J. Reiss, "Automatic equalization of multi-channel audio using cross-adaptive methods," in *Proc. AES 127th Conv.*, New York, NY, USA, Oct. 2009.

[19] Z. Ma, J. D. Reiss, and D. A. A. Black, "Implementation of an intelligent equalization tool using Yule–Walker for music mixing and mastering," in *Proc. AES 134th Conv.*, Rome, Italy, May 2013.

[20] P. Dutilleux, M. Holters, S. Disch, and U. Zölzer, "Filters and delays," in *DAFX: Digital Audio Effects*, U. Zölzer, Ed., 2nd ed. New York, NY, USA: Wiley, 2011, ch. 2, pp. 47–81.

[21] D. T. Yeh and J. O. Smith, "Discretization of the '59 fender bassman tone stack," in *Proc. Int. Conf. Digital Audio Effects (DAFx-06)*, Montreal, QC, Canada, Sep. 2006.

[22] L. Gabrielli, V. Välimäki, H. Penttinen, S. Squartini, and S. Bilbao, "A digital waveguide based approach for clavinet modeling and synthesis," *EURASIP J. Appl. Signal Process.*, vol. 2013, no. 1, pp. 1–14, May 2013.

[23] P. Regalia and S. Mitra, "Tunable digital frequency response equalization filters," *IEEE Trans. Acoust., Speech, Signal Process.*, vol. ASSP-35, no. 1, pp. 118–120, Jan. 1987.

[24] T. van Waterschoot and M. Moonen, "A pole-zero placement technique for designing second-order IIR parametric equalizer filters," *IEEE Trans. Audio, Speech, Lang. Process.*, vol. 15, no. 8, pp. 2561–2565, Nov. 2007.

[25] H. Behrends, A. von dem Knesebeck, W. Bradinal, P. Neumann, and U. Zölzer, "Automatic equalization using parametric IIR filters," *J. Audio Eng. Soc.*, vol. 59, pp. 102–109, Mar. 2011.

[26] J. D. Reiss, "Design of audio parametric equalizer filters directly in the digital domain," *IEEE Trans. Audio, Speech, Lang. Process.*, vol. 19, no. 6, pp. 1843–1848, Aug. 2011.

[27] S. Särkkä and A. Huovilainen, "Accurate discretization of analog audio filters with application to parametric equalizer design," *IEEE Trans. Audio, Speech, Lang. Process.*, vol. 19, no. 8, pp. 2486–2493, Nov. 2011.

[28] Motorola Inc., "Digital stereo 10-band graphic equalizer using the DSP56001," 1988, Application note.

[29] M. Holters and U. Zölzer, "Graphic equalizer design using higher-order recursive filters," in *Proc. Int. Conf. Digital Audio Effects (DAFx-06)*, Sep. 2006, pp. 37–40.

[30] S. Tassart, "Graphical equalization using interpolated filter banks," *J. Audio Eng. Soc.*, vol. 61, no. 5, pp. 263–279, May 2013.

[31] J. Rämö and V. Välimäki, "Optimizing a high-order graphic equalizer for audio processing," *IEEE Signal Process. Lett.*, vol. 21, no. 3, pp. 301–305, Mar. 2014.

[32] Z. Chen, G. S. Geng, F. L. Yin, and J. Hao, "A pre-distortion based design method for digital audio graphic equalizer," *Digital Signal Process.*, vol. 25, pp. 296–302, 2014.

[33] J. E. Lane, D. Hoory, and J. P. K. Brewer, "Method and apparatus for generating decoupled filter parameters and implementing a band decoupled filter," U.S. patent 5,687,104, Nov. 1997.

[34] B. Bank, "Direct design of parallel second-order filters for instrument body modeling," in *Proc. Int. Computer Music Conf.*, Copenhagen, Denmark, Aug. 2007, pp. 458–465 [Online]. Available: http://www.acoustics.hut.fi/go/icmc07-parfilt

[35] A. Härmä and T. Paatero, "Discrete representation of signals on a logarithmic frequency scale," in *Proc. IEEE Workshop Applicat. Signal Process. Audio Acoust.*, New Paltz, NY, USA, Oct. 2001, pp. 39–42.

[36] B. Bank, "Logarithmic frequency scale parallel filter design with complex and magnitude-only specifications," *IEEE Signal Process. Lett.*, vol. 18, no. 2, pp. 138–141, Feb. 2011.

[37] A. Härmä, M. Karjalainen, L. Savioja, V. Välimäki, U. K. Laine, and J. Huopaniemi, "Frequency-warped signal processing for audio applications," *J. Audio Eng. Soc.*, vol. 48, no. 11, pp. 1011–1031, Nov. 2000.

[38] T. Paatero and M. Karjalainen, "Kautz filters and generalized frequency resolution: Theory and audio applications," *J. Audio Eng. Soc.*, vol. 51, no. 1–2, pp. 27–44, Jan.–Feb. 2003.

[39] B. Bank, "Perceptually motivated audio equalization using fixed-pole parallel second-order filters," *IEEE Signal Process. Lett.*, vol. 15, pp. 477–480, 2008.

[40] B. Bank and G. Ramos, "Improved pole positioning for parallel filters based on spectral smoothing and multi-band warping," *IEEE Signal Process. Lett.*, vol. 18, no. 5, pp. 299–302, May 2011.

[41] J. A. Belloch, B. Bank, L. Savioja, A. Gonzalez, and V. Välimäki, "Multi-channel IIR filtering of audio signals using a GPU," in *Proc. IEEE Int. Conf. Acoust. Speech Signal Process.*, Florence, Italy, May 2014, pp. 6692–6696.

[42] L. Savioja, V. Välimäki, and J. O. Smith, "Audio signal processing using graphics processing units," *J. Audio Eng. Soc.*, vol. 59, no. 1/2, pp. 3–19, Jan.–Feb. 2011.

[43] B. Bank, "Audio equalization with fixed-pole parallel filters: An efficient alternative to complex smoothing," *J. Audio Eng. Soc.*, vol. 61, no. 1/2, pp. 39–49, Jan. 2013.

[44] T. W. Parks and C. S. Burrus, *Digital Filter Design*. New York, NY, USA: Wiley, 1987.

[45] F. B. Hildebrand, *Introduction to Numerical Analysis*, 2nd ed. New York, NY, USA: Dover Publications, Inc, 1987.

[46] R. A. Geiner and M. Schoesow, "Design aspects of graphic equalizers," *J. Audio Eng. Soc.*, vol. 31, no. 6, pp. 394–407, Jun. 1983.

[47] J. O. Smith, *Introduction to Digital Filters with Audio Applications,* W3K Publishing, 2007.

[48] A. V. Oppenheim and R. W. Schafer, *Digital Signal Processing*. Englewood Cliffs, NJ, USA: Prentice-Hall, 1975.

[49] J. Dattorro, "Effect design," *J. Audio Eng. Soc.*, vol. 45, no. 9, pp. 660–684, Sep. 1997.

[50] J. Rauhala, "The beating equalizer and its applications to the synthesis and modification of piano tones," in *Proc. 10th Int. Conf. Digital Audio Effects (DAFx-07)*, Bordeaux, France, Sep. 2007, pp. 181–188.

[51] V. Välimäki, J. S. Abel, and J. O. Smith, "Spectral delay filters," *J. Audio Eng. Soc.*, vol. 57, no. 7/8, pp. 521–531, Jul.–Aug. 2009.

[52] A. Pandey and V. J. Mathews, "Adaptive gain processing with offending frequency suppression for digital hearing aids," *IEEE Trans. Audio, Speech, Lang. Process.*, vol. 20, no. 3, pp. 1043–1055, Mar. 2012.

[53] J. Rämö, V. Välimäki, M. Alanko, and M. Tikander, "Perceptual frequency response simulator for music in noisy environments," in *Proc. AES 45th Int. Conf.*, Helsinki, Finland, Mar. 2012.

[54] A. Farina, "Simultaneous measurement of impulse response and distortion with a swept-sine technique," in *Proc. AES 108th Conv.*, Paris, France, Feb. 2000.

[55] U. Zölzer and T. Boltze, "Parametric digital filter structures," in *AES 99th Conv.*, New York, NY, USA, Oct. 1995.

[56] S. J. Orfanidis, "High-order digital parametric equalizer design," *J. Audio Eng. Soc.*, vol. 53, no. 11, pp. 1026–1046, Nov. 2005.

Jussi Rämö received his M.Sc. degree in communication engineering from the Helsinki University of Technology in 2009. His major subject was acoustics and audio signal processing.

Since 2009, he has worked as a researcher in the Department of Signal Processing and Acoustics at Aalto University, Espoo, Finland. Currently he is finalizing his Ph.D. degree in the field of headphone audio and digital signal processing. His research interests include sound reproduction and digital filtering.

Mr. Rämö is a member of the Audio Engineering Society. He was a member of the organizing committee of the Audio Engineering Society 51st International Conference on Loudspeakers and Headphones, Helsinki, Finland, August 2013.

Vesa Välimäki (S'90–M'92–SM'99) received the M.Sc. (Tech.), the Licentiate of Science in Technology, and the Doctor of Science in Technology degrees, all in electrical engineering, from the Helsinki University of Technology (TKK), Espoo, Finland, in 1992, 1994, and 1995, respectively. His doctoral dissertation dealt with fractional delay filters and physical modeling of musical instruments.

He was a Postdoctoral Research Fellow at the University of Westminster, London, U.K., in 1996. In 1997–2001, he was a Senior Assistant at the TKK Laboratory of Acoustics and Audio Signal Processing, Espoo, Finland. From 1998 to 2001, he was on leave as a Postdoctoral Researcher under a grant from the Academy of Finland. In 2001–2002, he was Professor of signal processing at the Pori unit of the Tampere University of Technology, Pori, Finland. He was appointed Docent in signal processing at the Pori unit of the Tampere University of Technology in 2003. In 2006–2007, he was the Head of the TKK Laboratory of Acoustics and Audio Signal Processing. He is currently Professor of audio signal processing in the Department of Signal Processing and Acoustics, Aalto University, Espoo, Finland. In 2008–2009, he was on sabbatical leave as a Visiting Scholar at the Center for Computer Research in Music and Acoustics (CCRMA), Stanford University, Stanford, CA.

Prof. Välimäki is a Fellow of the Audio Engineering Society, a Life Member of the Acoustical Society of Finland, and a Member of the Finnish Musicological Society. In 2000–2001, he was Secretary of the IEEE Finland Section. In 2008, he was the Chairman of DAFx-08, the 11th International Conference on Digital Audio Effects (Espoo, Finland). He was a Guest Editor for the *EURASIP Journal on Applied Signal Processing* and for the *EURASIP Journal on Advances in Signal Processing*, and was in the Editorial Board of the *Research Letters in Signal Processing* and of the *Journal of Electrical and Computer Engineering*. He is currently an Editorial Board Member of *The Scientific World Journal*. From 2005 to 2009 he was an Associate Editor of the IEEE SIGNAL PROCESSING LETTERS, and from 2007 to 2011 he was an Associate Editor of the IEEE TRANSACTIONS ON AUDIO, SPEECH, AND LANGUAGE PROCESSING. He was the Lead Guest Editor of a special issue of the IEEE SIGNAL PROCESSING MAGAZINE in 2007 and of a special issue of the IEEE TRANSACTIONS ON AUDIO, SPEECH, AND LANGUAGE PROCESSING in 2010. He is currently a Guest Editor of the special issue of the IEEE SIGNAL PROCESSING MAGAZINE on signal processing techniques for assisted listening. In 2007–2013 he was a Member of the Audio and Acoustic Signal Processing Technical Committee of the IEEE Signal Processing Society and is currently an Associate Member.

Balazs Bank (M'12) received his M.Sc. and Ph.D. degrees in electrical engineering from the Budapest University of Technology and Economics, Hungary, in 2000 and 2006, respectively. His doctoral dissertation was about physics-based synthesis of string instrument sounds with an emphasis on the piano.

In the academic year 1999/2000, he was with the Laboratory of Acoustics and Audio Signal Processing, Helsinki University of Technology, Finland. From 2000 to 2006 he was a Ph.D. student and research assistant at the Department of Measurement and Information Systems, Budapest University of Technology and Economics. In 2001 he visited the Department of Information Engineering, University of Padova. In 2007 he returned to the Acoustics Laboratory of Helsinki University of Technology for a year, with the support of an FP6 Marie Curie EIF individual fellowship. In 2008 he was with the Department of Computer Science, Verona University, Italy. In 2009–2010 he was a postdoctoral researcher at the Budapest University of Technology and Economics, supported by the Norway and EEA Grants and the Zoltán Magyary Higher Education Foundation. Currently, he is an associate professor at the Department of Measurement and Information Systems, Budapest University of Technology and Economics, Budapest, Hungary. His research interests include physics-based sound synthesis and filter design for audio applications.

Prof. Bank is a member of the Audio Engineering Society. Since 2013 he has been an Associate Editor of the IEEE SIGNAL PROCESSING LETTERS.